DR2005041

Data Repository Item 2005041: Equilibrium Line Altitude Reconstructions, Cosmogenic Surface-exposure Dating Methods, and Data Reduction

Equilibrium Line Altitude Reconstructions

The difference between the modern and paleo equilibrium line altitude (ELA) is used to estimate the severity of cooling that caused these glacial advances. The modern ELA is estimated from snow lines observed on the glaciers currently present in the basin (Figure DR1A). Estimates range from 1300 to 1700 m; accordingly we conservatively estimate the modern ELA to be ~1400 m. The paleo-ELA is estimated by using the accumulation-area ratio method. Paleo–glacier extents were digitally traced in a geographic information system over a digital elevation model (DEM) and a satellite image, which was then analyzed to generate a valley hypsometry curve (Figure DR1B). Based on an accumulation area ratio of 0.65 ± 0.05, a value adopted by many other researchers (Brugger and Goldstein, 1999, and references therein), we estimate a paleo-ELA of ~1100 m. A ~300 m drop in regional snowline at the time of moraine deposition represents a significant cooling event. For comparison the ELA depression at the time of the Last Glacial Maximum is estimated to be ~1000 m (Rabassa and Clapperton, 1990).

Cosmogenic Surface-exposure Dating Methods

Samples were collected by hand with hammer and chisel from large (0.2 to 1.5 m diameter) boulders at or near the moraine crest. The preferred boulder is one that has a wide flat surface that can be easily sampled, does not appear to have moved, or be weathering quickly (remnant glacial polish or sculpting is ideal), and has 20-30 % quartz

if sampling for ^{10}Be. Lithologies sampled were generally quartz-bearing rhyolite but also included granites and metamorphic rocks; ^{36}Cl was measured in two basalt samples. Some rocks were weathered and showed signs of spallation, but many preserved glacial sculpting or polish. The position and elevation of the samples was determined with a GPS and digital barometric altimeter respectively. There was good agreement between the altimeter and GPS elevations and we estimate a precision of ± 5 m for elevation measurements. The horizon shielding by the valley walls is characterized by several clinometer measurements and applied as a correction to production rates (see below).

Chemical isolation of ^{10}Be was performed at the University of Wisconsin-Madison following the methods of Bierman and others (2003), with only minor variations for some of the samples. For most samples, up to 100 g of quartz was separated from 1 to 2 kg of crushed rock by mechanical (magnetic and heavy liquid separation) and chemical (acid dissolution of non-quartz minerals) procedures. The quartz was cleaned in repeated etchings in a dilute solution of nitric and hydrofluoric acid to remove the outer rim of the quartz crystals and any meteoric ^{10}Be. After cleaning and a test to verify quartz purity, between 30 and 55 grams of quartz was dissolved in a mixture of concentrated hydrofluoric and nitric acids, along with a 500 μg spike of beryllium standard (Spex CertiPrep – Claritas PPT). A procedural blank for each batch of 11 samples is used to determine the amount of contaminant, non-cosmogenic ^{10}Be contained in the spike and other chemicals used in sample processing. After dissolution, beryllium was isolated from other trace impurities in the quartz through a series of selective chemical precipitations, as well as cation and anion exchange column separations. The Be is

oxidized, mixed with niobium metal, and packed into a target for accelerator mass spectrometry (AMS) analysis.

Chlorine was separated from whole rock samples following methods outlined in Stone and others (1996) at the Cosmogenic Isotope lab at the University of Washington. Ground samples were leached in hot, dilute nitric acid to remove meteoric ^{36}Cl. A sub sample was retained for major and trace element analysis (Table DR1). After weighing and addition of a chloride carrier-spike, the sample was dissolved in a warm mixture of concentrated hydrofluoric and nitric acid. AgCl was precipitated by addition of $AgNO_3$. Sulfur was removed by dissolution of the AgCl in dilute ammonia and precipitation as $BaSO_4$ (^{36}S is an isobaric interference on ^{36}Cl during AMS measurements). Pure AgCl was reprecipitated by acidification of the solution and loaded into targets for AMS analysis.

AMS analyses were conducted at PRIME Lab, Purdue University. ^{10}Be samples were measured against standards derived from NIST SRM 4325, and we accordingly increase ratios by 14% (keeping percent error constant) to correct for activity differences between this standard and those used at other AMS facilities. As cosmogenic production rates are determined empirically, knowledge of the exact activity of ^{10}Be is not necessary as long as there is robust intercalibration between standards (the basis of the 14% correction). ^{10}Be concentration in the quartz is determined by standard isotope dilution calculations from the amount of spike added to the sample and the blank corrected isotopic ratio (the blank ratio is subtracted from the sample ratio). ^{36}Cl concentration is determined by standard isotope dilution.

Cosmogenic Surface-exposure Age Calculations (Table DR2, DR3)

^{10}Be production rates are calculated according to Stone (2000) as the proximity to the Antarctic convergence leads to low air pressures and higher production rates in the region. Multi-decadal climate records in the region are sparse, but we estimate that mean annual sea level temperature is 285K and the mean annual sea level pressure is 1009.3 mb. A correction for modulation of production rate by changes in paleomagnetic intensity follow Nishiizumi et al., (1989) using the Sint-800 record of Guyodo and Valet (1999). The production rate is then scaled for sample thickness according to equations 3.78 and 3.81 of Gosse and Phillips (2001), and topographic shielding according to equation 6 of Dunne et al., (1999). We do not apply a correction for snow cover as the winter snow pack is generally thin and short lived.

^{36}Cl production rates are calculated using sea-level, high latitude values of 48.8 and 4.8 atoms gCa^{-1} yr^{-1} from spallation and muon capture reactions on Ca respectively (Stone et al., 1996, Stone et al., 1998), and 161 and 10.2 atoms gK^{-1} yr^{-1} from spallation and muon capture reactions on K respectively (Evans et al., 1997). Thermal and epithermal neutron capture rates are treated according to the method of Phillips et al. (2001). Sea-level, high latitude production rates are scaled to sample locations after Stone (2000) using atmospheric conditions described above. ^{36}Cl decay constant used is 2.303×10^{-6} yr^{-1}.

The exposure ages presented assume an erosion rate of 2 ± 2 mm/kyr. Kaplan et al. (2005) estimated erosion rate to be 1.5 ± 1.2 mm/kyr 100 km to the east of this area. We use a value that is slightly higher because this area is more humid, and we increase the uncertainty because of the extrapolation. Including erosion in the data reduction does

not significantly impact these ages; ^{10}Be boulder ages and uncertainties generally increase by about 1.5% and 3.5% respectively.

Uncertainties are calculated according to the General Rule presented in Taylor (1997; equation 3.47; partial differential of the age equation with respect to each of the variables) and includes analytic errors (weighing of sample, weighing and concentration of spike, and AMS error), as well as erosion rate and attenuation length uncertainty. All errors are reported at the 95% confidence level as to represent the full uncertainty in the age determinations. Uncertainties related to production rate scaling were not explicitly treated in the data reduction. These uncertainties are poorly constrained but thought to be better than 10% (Gosse and Phillips, 2001). As samples integrate production rate variability over their exposure history, young samples are more sensitive to high-frequency changes in the magnetic field of the Earth and Sun. Accordingly, we estimate that systematic production rate error for these samples may be closer to 10%; resulting in systematic age uncertainties of about 600 and 900 years for the inner and outer moraines respectively.

Replicate analyses were performed for five samples. Splits were isolated after crushing to ensure independent measurements, and no replicates were processed in the same batch. Two of these replicates are not reproducible at the 95% confidence level (FAC-02-16A/B and LBA-02-07A/B). We expect is fundamentally related to the very low amounts of cosmogenic nuclides in these samples caused by their youth and low elevations. ^{10}Be/Be ratios were on average only one order of magnitude higher than the procedural blank, and samples contain only about 1-5 million ^{10}Be atoms. Low ratios make AMS measurements very difficult, and relatively small sample sizes exacerbate the

problem. Replicate measurements are averaged to produce one age for each boulder (which are shown in Fig. 2). Note that using only the older or younger age for these two problematic replications does not change the overall interpretation of the moraine ages. Using the same outlier identification protocol defined below, using the younger ages leads to moraine ages of 6.2 ± 0.8 ka (with FAC-02-16A and FAC-02-12 excluded) and 8.3 ± 0.7 ka (FAC-02-05, FAC-02-13, and LBA-02-04 excluded) for the inner and outer moraine, respectively. Using only the older ages leads to ages of 6.5 ± 0.7 ka (FAC-02-12 excluded), and 8.8 ± 0.7 ka (FAC-02-13 and LBA-02-04 excluded) for the inner and outer moraine, respectively.

Cosmogenic Surface-exposure Data Interpretation

Four boulders were excluded from the weighted mean calculations because of potential inheritance problems. We make the fundamental assumption that the majority of the boulders reflect the timing of deposition (with random errors), but that some boulders will have non-random, geologic errors related to inheritance or exhumation problems, making the boulders anomalously older or younger than the others. Geologic outliers are identified on the basis of Chi-Square statistics and frequency distribution curves. The Chi-Square test is used to test the null hypothesis that the error distribution of the population is statistically different from random noise. Samples are rejected until population errors appear random. The bi-modal nature of the frequency distribution curves agrees with the Chi-Square analysis; the samples rejected during the Chi-Square analysis are the samples which form the secondary frequency maxima. Including all of

the samples in the weighted means calculations does not affect produce significantly different ages: 6.8 ± 1.8 and 9.3 ± 1.4 ka for the inner and outer moraine, respectively.

Such a high percentage of boulders with inheritance is somewhat unusual and is a departure from prior interpretive guidelines. Putkonen and Swanson (2003) reviewed data from 638 moraine boulders presented in 22 papers. Following the original interpretations of the authors, it was found that only 2% of the boulders were interpreted to have inherited isotopes, and that subsequent exhumation was a much more prevalent problem. Nevertheless, we feel justified in excluding these outliers. First, the samples that remain in the population have a well defined mean and show strong central tendency. Second, ice thinning during glacier retreat started at about 15 ka (Kaplan et al., 2004) exposing bedrock and boulders at the surface to cosmic rays. These glacial advances were much shorter and less severe than full glacial conditions (the focus of most of the chronology efforts reviewed in Putkonen and Swanson), so less material would have been eroded from the landscape causing boulders with inherited isotopes to comprise a greater percentage of the total volume of sediment in the moraine.

Data Repository References:

Bierman. P.R., Caffee, M.W., Davis. P.T., Marsella, K., Pavich, M., Colgan, P., Mickelson, D., and Larsen, J., 2003, Rates and timing of earth surface processes from in situ-produced cosmogenic Be-10, *in* Grew, E. S. ed., Beryllium: Mineralogy, Petrology, and Geochemistry, Reviews in Mineralogy and Geochemistry 50, p. 147-205.

Brugger, K.A., and Goldstein, B.S., 1999, Paleoglacier reconstruction and late Pleistocene equilibrium-line altitudes, southern Sawatch Range, Colorado, in Mickelson, D.M., and Attig, J.W., eds., Glacial processes past and present: Geological Society of America Special Paper 337, p. 103–112.

Brook, E.J., Brown, E.T., Kurz, M.D., Raisbeck, G., and Yiou, F., 1996, An Antarctic perspective on in-situ cosmogenic nuclide production: Radiocarbon, v. 38, p. 150.

Dunne, A., Elmore, D., Muzikar, P., 1999, Scaling factors for the rates of production of cosmogenic nuclides for geometric shielding and attenuation at depth on sloped surfaces: Geomorphology, v. 27, p. 3-11.

Evans, J.M., Stone, J.O., Fifield, L.K., and Cresswell, R.G., 1997, Cosmogenic chlorine-36 production in K-feldspar: Nuclear Instruments and Methods B, v. 123, p. 334-340.

Gosse, J.C., and Phillips, F.M., 2001, Terrestrial in situ cosmogenic nuclides: theory and application: Quaternary Science Reviews, v. 20, p. 1475-1560.

Guyodo, Y., and Valet, J. P., 1999, Global changes in intensity in the Earth's magnetic field during the past 800 kyr: Nature, v. 399, p. 249-252.

Holden, N.E., 1990, Total half-lives for selected nuclides: Pure and Applied Chemistry, v. 62, p. 941-958.

Kaplan, M.R., Ackert, R.P., Singer, B.S., Douglass, D.C., and Kurz, M.D., 2004, Cosmogenic nuclide chronology of milleneial-scale glacial advances during O-isotope stage 2 in Patagonia: Geological Society of America Bulletin, v. 116, p. 308-321.

Kaplan, M.R., Douglass, D.C., Singer, B.S., Ackert, R.P., and Caffee, M.W., 2005, Cosmogenic nuclide chronology of pre-last glaciation maximum moraines at Lago Buenos Aires, 46°S, Argentina: Quaternary Research.

Nishiizumi, K., Winterer, E.L., Kohl, C.P., Klein, J., Middleton, R., Lal., D., and Arnold, J.R., 1989, Cosmic ray production rates of 10Be and 26 Al in quartz from glacially polished rocks: Journal of Geophysical Research B, v. 94, p. 17,907-17,915.

Stone, J.O., 2000, Air pressure and cosmogenic isotope production: Journal of Geophysical Research B, v. 105, p. 23,753-23,759.

Stone, J.O., Allan, G.L., Fifield, K.L., and Cresswell, R.G., 1996, Cosmogenic chlorine-36 from calcium spallation: Geochimica Cosmchimica Acta, v. 60, p. 679-692.

Stone, J.O., Evans, J. M., Fifield, K.L., Allan, G.L., and Cresswell, R.G., 1998, Cosmogenic chlorine-36 production in calcite by muons: Geochimica Cosmchimica Acta, v. 62, p. 433-454.

Phillips, F.M., Stone, W.D., and Fabryka Martin, J.T., 2001, An improved approach to calculating low-energy cosmic-ray neutron fluxes near the land/atmosphere interface: Chemical Geology, v. 175, p. 689-701.

Putkonen, J., and Swanson T., 2003, Accuracy of cosmogenic ages for moraines: Quaternary Research, v. 59, p. 255-261.

Rabassa, J. and Clapperton, C.M., 1990, Quaternary glaciations of the Southern Andes: Quaternary Science Reviews, v. 9, p. 153-174.

Taylor, J.R., 1997, An Introduction to Error Analysis, The Study of Uncertainties in Physical Measurements 2nd ed.: Sausalito, CA, University Science Books, 327 p.

Table DR1. Composition data for Fachinal moraine boulders.

Sample ID	SiO_2	Al_2O_3	CaO	MgO	Na_2O	K_2O	Fe_2O_3	MnO	TiO_2	P_2O_5	Cr_2O_3	U	Th	Gd	Sm	B
	%	%	%	%	%	%	%	%	%	%	%	ppm	ppm	ppm	ppm	ppm
PAT-98-073	57.55	15.36	6.29	2.98	2.38	1.78	8.79	0.15	1.15	0.21	0.03	1.93	9.4	5.11	5.8	66
PAT-98-075	54.22	17.05	2.74	2.84	4.53	2.07	10.23	0.28	0.88	0.26	0.02	1.01	4.7	3.85	3.9	41

Table DR2: ^{10}Be data from moraine boulders on Fachinal moraines

Sample ID	Lithology	Boulder height(m)	Boulder diam (m)	Thickness (cm)	Lat. (°S)	Long. (°W)	Altitude m asl	Mass Quartz	^{10}Be Conc. 10^4 at $g^{-1} \pm 2\sigma$	Prod. Rate at g^{-1} yr^{-1}	Exposure Age 2σ error
FACHINAL INNER											
FAC-02-04	Rhyolite	1.0	1.5	2.5	46.569	72.212	335	50.546	4.33 ± 0.90	7.01	6.3 ± 1.3
FAC-02-10	Granite	1.0	1.1	2	46.571	72.238	343	31.849	3.99 ± 4.34	7.10	5.7 ± 6.3
FAC-02-12	Vein Qtz	0.3	0.4	5	46.570	72.237	343	48.808	6.89 ± 1.20	6.85	10.3 ± 1.8
FAC-02-16A	Rhyolite	0.4	0.5	2.5	46.570	72.237	348	47.934	2.77 ± 0.86	7.09	3.9 ± 1.3
FAC-02-16B	Rhyolite	0.4	0.5	2.5	46.570	72.237	348	41.220	5.40 ± 1.08	7.09	7.7 ± 1.6
FAC-02-18	Rhyolite	0.4	0.8	3	46.573	72.206	345	47.912	4.56 ± 0.80	7.04	6.6 ± 1.2
FAC-02-20	Rhyolite	1.0	1.8	5	46.572	72.207	340	35.765	3.53 ± 1.38	6.90	5.2 ± 2.0
FACHINAL OUTER											
FAC-02-02	Rhyolite	1.0	1.8	2.5	46.568	72.211	323	20.907	5.27 ± 1.66	6.91	7.8 ± 2.5
FAC-02-05	Rhyolite	1.5	2.0	4.5	46.567	72.214	337	49.338	8.13 ± 1.62	6.89	12.1 ± 2.5
FAC-02-13	Granitoid	1.0	1.1	6.5	46.568	72.236	351	52.064	8.71 ± 1.54	6.85	13.1 ± 2.4
LBA-02-04	Rhyolite	1.1	1.3	5	46.571	72.203	336	19.340	10.09 ± 2.22	6.85	15.2 ± 3.5
LBA-02-05A	Rhyolite	0.3	0.5	5	46.570	72.204	343	46.895	7.48 ± 1.84	6.89	11.1 ± 2.8
LBA-02-05B	Rhyolite	0.3	0.5	4	46.570	72.204	343	33.000	5.14 ± 1.14	6.95	7.5 ± 1.7
LBA-02-06A	Rhyolite	1.3	2.0	5	46.569	72.205	337	36.241	5.90 ± 1.46	6.85	8.8 ± 2.2
LBA-02-06B	Rhyolite	1.3	2.0	4	46.569	72.205	337	46.989	4.93 ± 0.98	6.91	7.3 ± 1.5
LBA-02-07A	Rhyolite	1.3	2.5	5	46.569	72.206	338	44.137	4.45 ± 1.34	6.85	6.6 ± 2.0
LBA-02-07B	Rhyolite	1.3	2.5	4	46.569	72.206	338	47.487	7.48 ± 1.36	6.92	11.1 ± 2.1
LBA-02-08A	Rhyolite	1.5	2.0	5	46.569	72.207	340	59.163	5.43 ± 0.80	6.87	8.0 ± 1.2
LBA-02-08B	Rhyolite	1.5	2.0	4	46.569	72.207	340	35.325	7.08 ± 1.32	6.93	10.4 ± 2.0

Table notes: Age equation used is $t = (-1/(\lambda + E/L))*[\ln(1-N(\lambda + E/L)/P)]$; where N is ^{10}Be concentration, P is production rate, E is 2±2 mm/kyr expressed as g cm^{-2} y^{-1}, λ is the decay constant (4.56±0.15 E-07; Holden,1990), and L is the attenuation length (145±7 g cm^{-2}; Brook et al., 1996). Topographic shielding for these samples is less than 1 %). Procedural blanks contains 1.0 to 2.7 x 10^5 atoms ^{10}Be (^{10}Be/Be of 3-8 x10^{-15}); typically ~10% of total ^{10}Be content.

Table DR3: ^{36}Cl exposure ages of Fachinal moraine boulders

Sample	Lithology	Boulder height (m)	Boulder diam (m)	Thickness (cm)	Lat. (°S)	Long. (°W)	Altitude m asl	Ca %	K %	[Cl] ppm	$\sigma_{35}N_{35}/\Sigma$ [1]	^{36}Cl conc [2] 10^4 at $g^{-1} \pm 2\sigma$	Exp Age 2σ error
FACHINAL OUTER													
PAT-98-073	Basalt	0.2	0.3	2.5	46.573	72.242	320	4.50	1.48	264	0.0162	16.0 ± 4.8	9.2 ± 3.0
PAT-98-075	Basalt	0.2	0.3	2.0	46.577	72.244	320	1.96	1.72	88	0.00585	8.33 ± 2.0	8.9 ± 2.3

Table notes: [1] Fraction of thermal neutrons captured by ^{35}Cl. [2] Corrections for radiogenic ^{36}Cl are 34% for PAT-98-073 and 15% for PAT-98-075. Procedural blank contain <6 x 10^3 atoms ^{36}Cl (^{36}Cl/Cl < 10^{-15}).

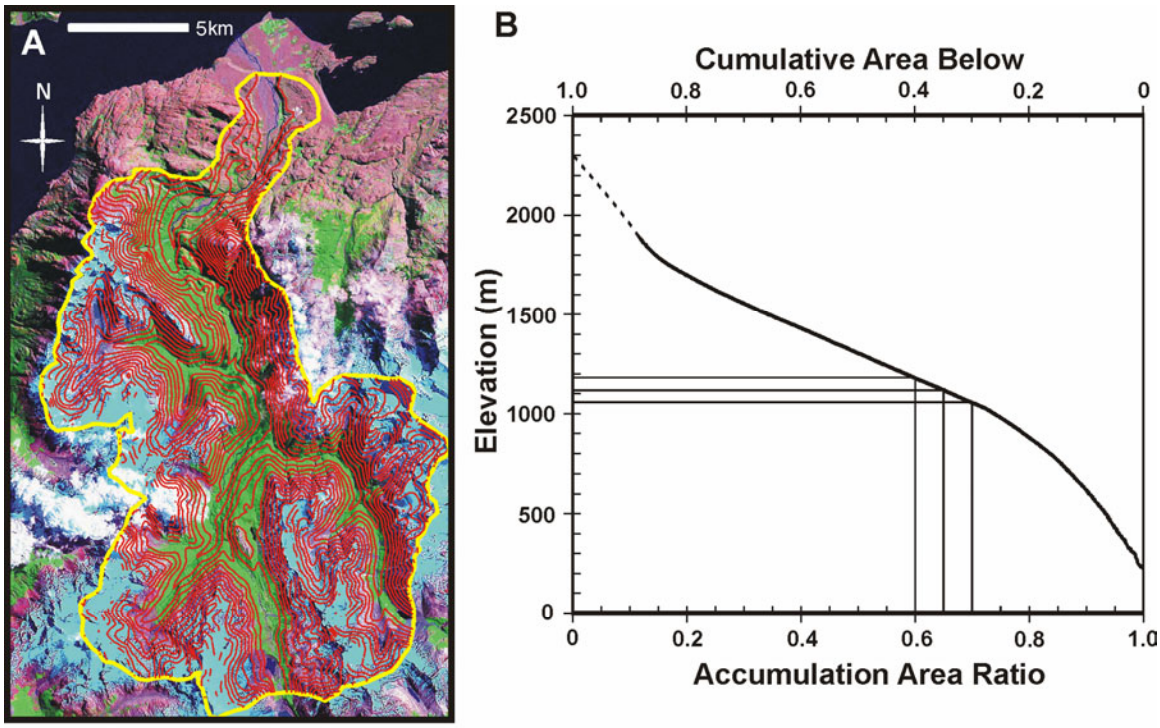

Figure DR1
Douglass et al., Geology

Figure DR1: A: Landsat 7 ETM (Bands 7, 2, 3) and outline of glacier valley (in yellow). Elevation contours (100 m contour interval) from Shuttle Radar Topography Mission data (SRTM) are shown in red. B: Valley hypsometry curve with envelope for an accumulation area ratio of 0.65 ± 0.05. The upper part of the hypsometry curve is dashed because of "holes" in the DEM over steep snow covered slopes.